


Economic optimization for a dual-feedstock lignocellulosic-based sustainable biofuel supply chain considering greenhouse gas emission and soil carbon stock

Bingquan Zhang[†] , Energy and Sustainability Research Institute Groningen, University of Groningen, Groningen, The Netherlands; Center for Industrial Ecology, Yale University, New Haven, CT, USA
Changqiang Guo[†], **Tao Lin**, College of Biosystems Engineering and Food Science, Zhejiang University, Hangzhou, China
André P. C. Faaij, Energy and Sustainability Research Institute Groningen, University of Groningen, Groningen, The Netherlands; Netherlands organization for Applied Scientific Research - TNO Energy Transition, Utrecht, The Netherlands

Received July 01 2021; Revised January 10 2022; Accepted January 24 2022;

View online April 11, 2022 at Wiley Online Library (wileyonlinelibrary.com);

DOI: 10.1002/bbb.2347; *Biofuels, Bioprod. Bioref.* 16:653–670 (2022)



Abstract: Environmental factors, including greenhouse gas (GHG) emissions and soil organic carbon (SOC), should be considered when building a sustainable biofuel supply chain. This work developed a three-step optimization approach integrating a geographical information system-based mixed-integer linear programming model to economically optimize the biofuel supply chain on the premise of meeting certain GHG emission criteria. The biomass supply grid cell was considered first, based on a maximum level of GHG emissions, prior to economic optimization. The optimization simultaneously considered dual-feedstock sourcing, selection between distributed and centralized configurations, and the impact of maintaining SOC balance in agricultural soil on biomass availability. The applicability of the modeling approach was demonstrated through a case study that optimized a dual-feedstock renewable jet fuel supply chain via a gasification-Fischer-Tropsch (gasification-FT) conversion pathway in 2050 under three biomass availability scenarios. The case study results show that the differences in procurement costs and GHG emissions between energy crops and agricultural residues have a large impact on the layout of the supply chain. The supply-chain configuration tends to be more centralized with large-scale biorefineries when a supply region has an intensive and centralized distribution of biomass resources. The cost-supply curves demonstrated the technical potential of biofuels that could be obtained at a certain level of cost. Additionally, sensitivity analysis shows that the GHG emission credit from producing extra electricity

Correspondence to: Bingquan Zhang, Center for Industrial Ecology, Yale University, 380 Edwards St, New Haven, 06511, CT, USA, E-mail: bingquan.zhang@yale.edu; or Tao Lin, College of Biosystems Engineering and Food Science, Zhejiang University, Hangzhou, China. E-mail: lintaot1@zju.edu.cn

[†]B. Zhang and C. Guo contributed equally to this work.

© 2022 The Authors. *Biofuels, Bioproducts and Biorefining* published by Society of Industrial Chemistry and John Wiley & Sons Ltd. This is an open access article under the terms of the Creative Commons Attribution NonCommercial License, which permits use, distribution and reproduction in any medium, provided the original work is properly cited and is not used for commercial purposes.

during the gasification-FT process will be significantly reduced with a rising share of renewable electricity generation in the future. © 2022 Society of Chemical Industry and John Wiley & Sons, Ltd

Supporting information may be found in the online version of this article.

Key words: biofuel supply chain optimization; GHG emission; lignocellulosic biomass; mixed integer linear programming; soil organic carbon; sustainable

Introduction

For decades, biofuel has been utilized as a type of renewable energy alternative to fossil fuel mitigate greenhouse gas (GHG) emissions. As the main output products of the lignocellulose-based conversion technologies, advanced biofuels such as bioethanol, biodiesel, biobutanol, and renewable jet fuel (RJF) could be utilized in the transport sector in the medium to long term.^{1,2} The International Energy Agency (IEA) has estimated that the primary demand for bioenergy would account for 9.1%, 10.3%, and 12.3% of total global primary energy demand in 2040 under the ‘current policies scenario’, ‘stated policies scenario’, and ‘sustainable development policies scenario’, respectively.³ To achieve the goals of sustainable development and mitigation of global climate change, it is important to increase the share of biofuels in the future energy mix, and the successful production of biofuels depends heavily on a secure supply chain.

The supply chain of the biomass-to-biofuels industry is full of uncertainties, such as the scattered distribution of biomass supply sites, uncertain availability of biomass resources, and logistical problems.^{4–6} It is therefore crucial to carry out strategically economic optimization of the biofuel supply chain to tackle such uncertainties and realize large-scale biofuel production. Many studies have been performed on the economic optimization of the biofuel supply chain using mixed integer linear programming (MILP) models based on geographic information systems (GIS).⁷ The GIS-based optimization model allows the locations of biomass supply sites, storage and pretreatment (SP) and biorefinery (BR) facilities to be identified, as well as possible routines with the shortest distance between transport networks.⁸ A few studies have developed and applied a GIS-based MILP model called BioScope to minimize the total cost of biofuel supply chains with various feedstocks and conversion pathways.^{9–13}

Environmental performance, including GHG emissions and soil health, needs to be taken into account in supply chain optimization. To achieve global or regional GHG mitigation targets by replacing fossil fuels with biofuels,

the production of biofuels has to follow GHG emission regulations. The EU Renewable Energy Directive and the US Renewable Fuel Standard both stipulate a GHG emission reduction threshold of 60% for lignocellulosic-based biofuels in comparison with the fossil fuel baseline.^{14,15} Hence it is necessary to find ways to optimize the biofuel supply chain economically within such regulatory frameworks. To identify possible biomass supply regions where GHG reduction potential is lower than the threshold in a biofuel supply chain, it is necessary to calculate the unit GHG emission from each biomass supply region. Many studies have used the ϵ -constraint method to create the pareto-optimal curves revealing the trade-off between economic and environmental performance.^{12,16–23} However, when the cost optimization of the biofuel supply chain is carried out on the premise of reaching a certain GHG reduction criterion, the ϵ -constraint method cannot solve this problem efficiently because creating the pareto-optimal curves is time-consuming and not necessary. Furthermore, most of these studies were carried out with a county-level or above. They failed to calculate the unit biofuel production cost and GHG emission on a grid cell basis at a high spatial resolution and did not adequately analyze the spatial variations in the unit biofuel production cost and GHG emission.

In addition to GHG emissions, the biomass supply faces uncertainties from the perspective of maintaining soil health, which is important for building a sustainable biofuel supply chain because the excessive removal of agricultural residues for biofuel production might come at the cost of reduced soil quality.^{20,24} Some studies have shown that residues are important contributors to maintain soil organic carbon (SOC) and could prevent soil erosion.^{25–27} Appropriate land management, such as conservation tillage, could significantly reduce the decomposition of SOC.²⁸ Consequently, maintaining high SOC content may require a large volume of residues to be retained in the soil, thus reducing the removal rate of residues for biofuel production.²⁹ Furthermore, agricultural residues are valuable as feedstocks for producing animal feed, industry materials, bio-chemicals, and mushroom matrix. The competing uses of agricultural residues add great uncertainty to supply.²⁹ Hence, the supply

potential of agricultural residues for biofuel production would depend on the SOC level being maintained, land management being implemented, and the competing use of agricultural residues. Besides, the commercial production of perennial lignocellulosic energy crop from marginal land has not yet appeared in many countries. Thus, the supply of energy crop in the future may change with time, policies, and marginal land availability. The uncertainty of biomass supply affects the optimal design of the biofuel supply chain. Moreover, differences in procurement costs and GHG emissions between agricultural residues and energy crops can have a great impact on the economic and GHG performances of the biofuel supply chain.^{29,30} The uncertainty of the biomass feedstock supply and dual-feedstock sourcing from the same region should be considered in the optimization.

To the best of our knowledge, no comprehensive work has been conducted on a grid cell-based optimization of the biofuel supply chain where the economic objective is achieved by simultaneously meeting certain criteria for GHG emission reduction and considering soil health and the uncertainty of biomass supply. To fill the research gap, this study proposes a three-step MILP-based modeling approach that can design an economically optimal biofuel supply chain strategically on a spatial grid cell basis on the premise of reaching a certain GHG reduction criterion and maintaining soil health. The overall structure of this approach is presented in Fig. 1. Considering the strong demand for biofuel in the future, the approach was built based on the assumption that all biomass resources are selected in the biofuel supply chain. This study is differentiated from other works by simultaneously incorporating the following specific characteristics: (1) the impact of GHG emissions on the economic optimization of the biofuel supply chain quantified by setting a certain GHG reduction criterion; (2) the impacts of maintaining soil health, different combinations of biomass resources, and competing uses of agricultural residues on biomass availability; (3) the selection of distributed and centralized supply chain configurations; (4) the unit production cost and GHG emission of the optimal supply chain on a grid

cell basis, which are calculated by the model. This approach was applied to a case-study in the Jing-Jin-Ji region of North China under three biomass availability scenarios.

Methodology

Biomass supply

Agricultural residues from cropland and perennial energy crops from marginal land are selected as feedstocks for biofuel production due to their potential availability and because they are no threat to food security. However, the uncertainty of biomass availability mentioned above should be considered. This work considered several biomass availability scenarios comprehensively (see below) considering SOC balance, different feedstock combinations, and competing use of agricultural residues.

A method developed by Zhang et al. (2021)²⁹ was used to calculate the volume of agricultural residues collectible for biofuel production at different SOC levels. The theoretical quantity of residues is first estimated according to the yields of crop products, the residue-to-product ratio, and the root-shoot ratio. Then the volume of returned residues for maintaining the target SOC level is calculated by the RothC soil carbon model. Finally, the quantity of collectible residues available for biofuel production is calculated by subtracting the returned volume from the theoretical volume of residues.

Modeling framework

The model used for supply chain optimization is adapted from the BioScope model,^{9–12} whose purpose is to develop a biofuel supply chain consisting of three consecutive echelons, i.e. biomass feedstock supplying region, SP, and biorefinery, taking the lowest cost as objective function. The location and capacity of facilities and the flux of biomass between echelons are key decision variables. The original BioScope model aims to design a distributed supply-chain configuration in which

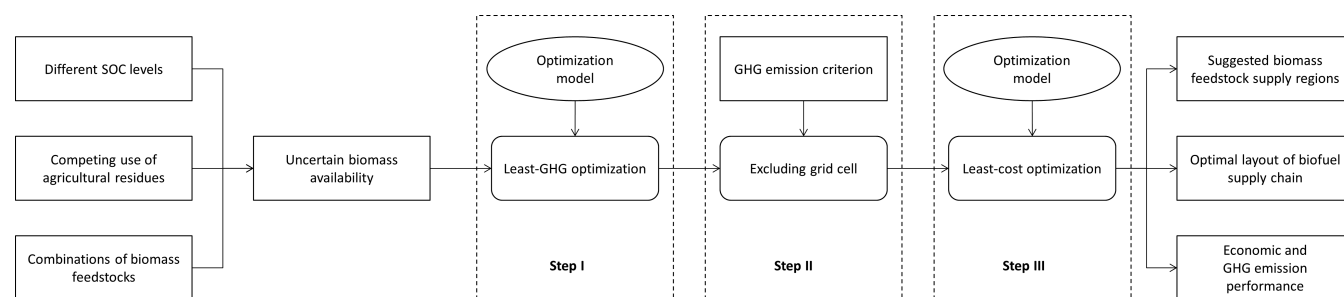


Figure 1. Overall structure of the three-step optimization of the sustainable biofuel supply chain considering GHG emission criterion and uncertain biomass availability.

biomass commodity can only be transported from the supply region to the SP and then to the biorefinery assuming there is no preprocessing facility for raw biomass in the terminal biorefinery. However, in the present study, environmental emissions were added to the objective function of the improved BioScope model. By allowing the biomass feedstock to be transported directly from supply region to biorefinery, the BioScope model was also improved so that it can construct a hybrid supply-chain system, which can integrate distributed and centralized structures. The improved model was developed on the Spyder platform using Python 3.7 and solved by Gurobi 9.0.3. Its framework is presented in Fig. 2. The total GHG emissions (Z_1) and total annual supply cost (Z_2) of the biofuel supply chain are minimized by using the following objective functions Eqn (1, 2), respectively. Model constraints, detailed formulas, and nomenclature are presented in Appendix A.

$$\min Z_1 = \alpha E_B + E_T + E_S + E_F \quad (1)$$

$$\min Z_2 = \beta(C_B + C_T + C_S + C_F) \quad (2)$$

The improved model enables dual-feedstock sourcing when two types of feedstocks with different yields, procurement costs, and provision GHG emissions are located within the same region, and choosing the optimum configuration between the distributed and centralized modes. The decision variables including biomass flow and the optimal numbers, location, and capacities of SP and biorefinery facilities are determined by the model.

To run the model, spatially gridded data include the supply volume, procurement cost, and GHG emission of feedstock provision, the potential locations of SP and biorefinery, and the road network are required (Fig. 2). The techno-economic and GHG emission-related parameters include SP and the biorefinery-related parameters and transportation-related parameters (Fig. 2). The SP and biorefinery-related parameters include capital expenditure (CAPEX) for SP and biorefinery, variable operational expenditure (OPEX) for SP

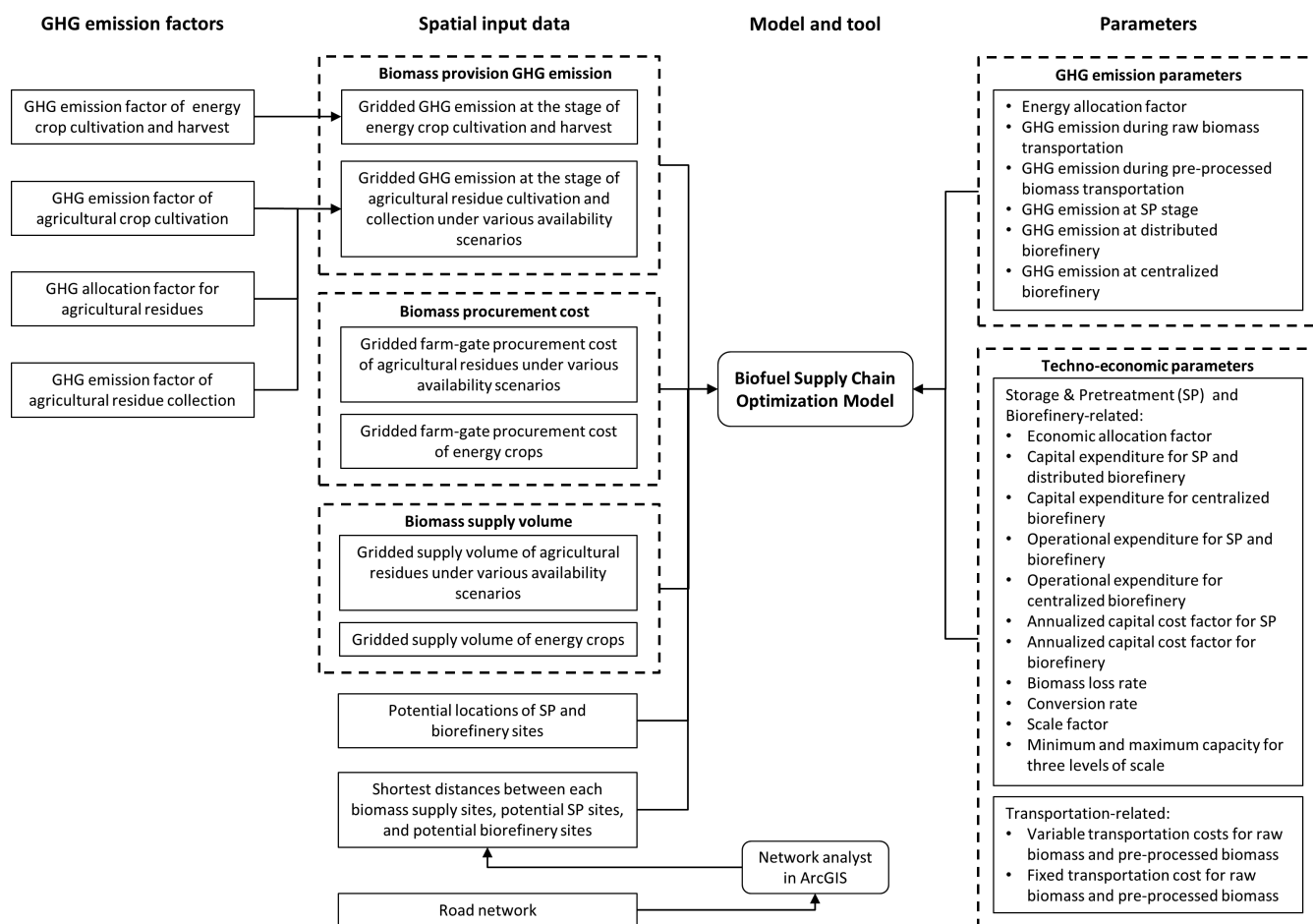


Figure 2. The framework, parameters, and data flow of the biofuel supply chain optimization model.

and biorefinery, CAPEX-dependent OPEX, annuity factors for annualized CAPEX calculation, conversion rates of SP and biorefinery process, and economic allocation factor for biofuel. The impact of economies of scale on capital-related costs presented a power law,³¹ and the non-linear power law was approximated by a three-stage piecewise linear function,⁹ as shown in Appendix B (Figure B1). The transportation distance was pre-optimized. The shortest distance between any two sites was selected by running the Network Analyst of ArcGIS. The GHG emissions accrue at the stages of crop cultivation, feedstock on-farm collection and harvest, transportation, pretreatment, and biorefinery.

Optimization procedure

Greenhouse gas emission criteria are set to exclude grid cells (biomass supply site) that have a high GHG emission of biofuel production to conduct economic optimization while taking into account specific environmental constraints. For instance, if a 70% reduction of GHG emission of biofuel production compared to fossil fuel is considered to be a sustainable criterion, it means that grid cells with a GHG reduction potential of lower than 70% will be excluded from the original biomass supply sites. The whole optimization is carried out as the following steps:

- Step I. Estimating the minimum GHG emission of the supply chain on a grid-cell basis using the improved BioScope model by minimizing the total GHG emissions as the objective, using Eqn (1).
- Step II. Excluding grid cells that have a GHG emission of biofuel production higher than the GHG emission criterion from the original biomass supply sites, and keeping the rest of the grid cells for further economic optimization.
- Step III. Conducting economic optimization of the biofuel supply chain by minimizing the total production cost as the objective, using Eqn (2).

Case study

Design of the case study

The Jing-Jin-Ji district, known as the Beijing-Tianjin-Hebei metropolitan region of China, was selected as the case study region. The reasons for choosing the region are: (1) the lignocellulosic biomass resources are substantial,^{29,30,32} (2) a huge jet fuel consumption potential exists because it is the biggest urbanized megalopolis region in north China with a total population of 112 million people and the second-largest airport cluster in China; (3) the strong advantages to biofuel production and consumption as the region has traditionally been involved in heavy industries, manufacturing, petrochemical sectors, aviation, and logistics.

Previous studies show that there is a huge availability potential of lignocellulosic biomass for biofuel production in China, and they estimated that up to 888 Mt of agricultural residues are theoretically collectible at an on-farm collection cost below 17.6 \$·Mg⁻¹ in 2050, and 1644 Mt of *Miscanthus* and switchgrass from marginal land are available for biofuel production at a farm-gate production cost below 65.1 \$·Mg⁻¹ in 2050.^{29,30,32}

Renewable jet fuel is selected as the target product in this study as GHG emissions from the commercial aviation industry have increased rapidly with the growth in demand for air travel and air cargo over the past decades globally. Using lignocellulosic biomass as feedstock for RJF production could be realized by Fischer–Tropsch (FT), hydrothermal liquefaction (HTL), pyrolysis, alcohol-to-jet (ATJ), and direct sugars to hydrocarbons (DSHC) technologies.³³ Comprehensively considering the GHG emission performance and economic assessment, the gasification-FT technology is selected as the conversion technology among the five technologies for RJF production as it achieves the lowest GHG emissions,³³ which is specifically important

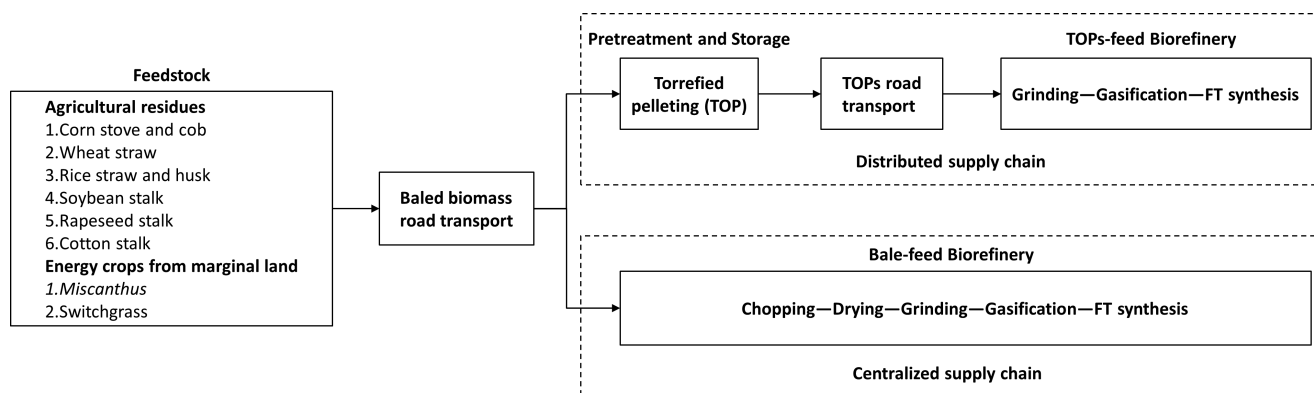


Figure 3. Design of a three-stage renewable jet fuel supply chain.

for its market competitiveness when carbon policies are introduced in the future.^{12,34} For the gasification-FT jet fuel production, the torrefied pellets (TOPs) are selected as the output of pretreatment and the feedstock fed to the gasification process in this study.^{35,36}

The design of the RJF supply chain with various biomass feedstocks and supply chain configurations is shown in Fig. 3. In the distributed configuration, baled biomass is pre-processed to TOPs by torrefaction technology at the storage and pretreatment (SP) facility, and then the TOPs are transported to the TOPs-feed biorefinery plant. In the centralized configuration, baled biomass is transported directly to the bale-feed biorefinery plant instead of the SP facility. The gasification process in this study is operated at a high temperature of 1300 °C by using a pressured, oxygen-blown, and entrained-flow-based gasifier.³⁷ Although there are many kinds of gasification-FT equipment and technical routes,^{38–40} it is not the objective to evaluate all of them in this case study. It is assumed that jet fuel is the main product and naphtha is the by-product of the gasification-FT conversion pathway with a product to by-product ratio of 3.4:1 except for electricity.³³ The three levels of biomass input capacity for SP and biorefinery facilities were assumed to be 50 000–600 000 Mg·year⁻¹, 600 000–1 300 000 Mg·year⁻¹, and 1 300 000–2 000 000 Mg·year⁻¹ for small, medium, and large scale, respectively. A scaling factor of 0.7 was used for the estimation of total capital expenditure.

The GHG emission criterion was set to be a 70% reduction in the GHG emissions from biofuel production compared to fossil fuel in this case study. This criterion is higher than the highest GHG reduction threshold (60%) for biofuels from two prominent regulatory frameworks, the EU Renewable Energy Directive and the US Renewable Fuel Standard.^{14,15} A life-cycle GHG emission factor of 86 kg CO_{2-eq}·GJ⁻¹ for fossil fuel is used in this study,⁴¹ thus the GHG emission criterion with a 70% reduction in GHG emission compared to fossil fuel is calculated to be 25.8 kg CO_{2-eq}·GJ⁻¹ for biofuel production.

Scenario

To explore the future (2050) optimal layouts and minimize the cost of the RJF supply chain under scenarios from the minimum to the maximum biomass availability, we established three scenarios (Min, Inter, and Max) by combining various elements that affect biomass availability. These elements include the combination of biomass feedstock, SOC stock and land management, and competing demands of agricultural residues for alternative use.

A previous study calculated the volume of agricultural residues required to be retained in the soil to maintain certain target SOC levels at equilibrium status in China

Table 1. Definitions of the SOC and land management scenarios and BASE scenario.²⁹

Scenarios	Definition
IHSS	A certain amount of agricultural residue is required to remain in the soil to maintain a target SOC level of 2% or more with the implementation of no-till cultivation (I) and increased crop yield by 2050 (II).
Base	No agricultural residues are required to remain in the soil, no target SOC level is set, and all theoretical amounts of agricultural residues could be removed from the field with increased crop yield by 2050.

I No-tillage cultivation is implemented to all the arable land in China to increase the SOC level by 1.23 for tropical moisture climate, 1.17 for the tropical dry climate, 1.16 for temperate moisture climate, and 1.10 for the temperate dry climate.
II Crop productivity increase by a certain increase rate by 2050 as agricultural technology is improved while considering possible climate change in 2050.

under different SOC and land-management scenarios, which are called the improved high SOC scenario (IHSS) and the base scenario.²⁹ The detailed scenarios are depicted in more detail in Table 1. The SOC stock and land management are not considered for energy crops in this study, because the cultivation of perennial herbaceous energy crops has very limited negative impacts or even positive impacts on the SOC stock of marginal land and it is hard to quantify the overall SOC stock change due to the land-use change from marginal land to land for energy-crop cultivation.^{42–45} Biomass availability scenarios with combinations of multiple elements are shown in Table 2. It is assumed that the RJF demand in 2050 will be very large, and the RJF production under each scenario is constrained by the supply potential of all available biomass resources.

Input data

Spatial input data

The spatial data include gridded data of feedstock supply volume and procurement cost, GHG emission of feedstock provision, potential locations of SP and biorefinery, and road networks. The spatial distributions of production and procurement cost of energy crops are originally at 1 × 1 km resolution from the previous studies.^{30,32} Then all these spatial data were aggregated at a 25 × 25 km spatial resolution. We assumed that the locations of feedstock supply, SPs and biorefineries fall in the center of the 25 × 25 km grid cells (Figure B2 in Appendix B). The road network layer used in the network analysis was extracted from the 1:1 000 000 National Basic Geographical Database, which was derived from the National Catalogue Service for Geographic

Table 2. Biomass availability scenarios with combinations of multiple elements.

Scenarios	Agricultural residues			Energy crops
	IHSS	Base	Competing use	
Minimum biomass supply (Min)	√			
Intermediate biomass supply (Inter)		√	√	√
Maximum biomass supply (Max)		√		√

Information.⁴⁶ The acquisition of the spatial data of biomass provision GHG emissions is described below.

Techno-economic parameters

The case study-specific techno-economic parameters, including SP-, biorefinery- and transportation-related parameters are shown in Table 3. The scale parameters of CAPEX for SP, bale- and TOPs-feed gasification-FT plants are shown in Tables 4–6.

Greenhouse-gas emission-related data and parameters

The GHG emissions at the crop-cultivation stage are derived from applications of fertilizers, pesticides, machinery, irrigation, methane from rice paddies, and other activities.

For the agricultural crops, the detailed calculation of GHG emission from the crop cultivation stage is shown in Appendix C. The spatial data of GHG emission per unit of collectible residue at the cultivation and on-farm collection stage under different biomass availability scenarios are shown in Figure B3 in Appendix B.

For energy crops, the GHG emissions from *Miscanthus* and switchgrass on-farm production and harvest are assumed to be the same and calculated to be 625 kg CO_{2-eq}/ha according to the data from Felten et al. (2013).⁴⁸ Then the spatial distribution of GHG emission per unit of energy crop at the stage of cultivation and harvest are generated based on the previous study³² and shown in Figure B3 in Appendix B. Other data of GHG emissions from transportation, pretreatment, and biorefinery are summarized in Table 7.

Results and discussion

Environmental optimization

The results from the first-step environmental optimization are demonstrated by GHG-supply curves (Fig. 4). Under the Min scenario, almost all jet fuel (19 PJ) is supplied at a unit GHG emission of less than 25.8 kg CO_{2-eq}-GJ⁻¹. For the Inter and max scenarios, around 240 PJ and 290 PJ of jet fuels could be supplied applied at a unit GHG emission of less than 25.8 kg CO_{2-eq}-GJ⁻¹, respectively. Grid cells with unit GHG emission

Table 3. Techno-economic parameters.

Description	Value	Source
Economic allocation factor for jet fuel	0.82 ^a	33
Annualized capital cost factor for SP facility	0.117	13,35
Annualized capital cost factor for biorefinery facility	0.121	12
Biomass loss rate at the SP or bale-feed biorefinery	0.05	12
Conversion rate from biomass to jet fuel	0.18 Mg fuel/Mg biomass	33
Conversion rate from biomass to TOPs	0.791 Mg TOPs/Mg biomass	47
Conversion rate from TOPs to jet fuel	0.228 Mg fuel/Mg biomass	33
Variable transportation cost of raw biomass (bale)	0.15 \$/Mg biomass/km	9,59
Variable transportation cost of pre-processed biomass (TOPs)	0.06 \$/Mg biomass/km ^b	-
Fixed transportation cost of raw biomass (bale)	5.42 \$/Mg biomass	9,59
Fixed transportation cost of pre-processed biomass (TOPs)	2.17 \$/Mg biomass ^b	-
Total variable OPEX for SP	10.25 \$/Mg biomass	35,47
Total variable OPEX for bale-feed biorefinery	10 \$/Mg biomass	12
Total variable OPEX for TOPs-feed biorefinery	0.56 \$/Mg biomass ^c	12,37
CAPEX-dependent OPEX	0.102* CAPEX/capacity ^d	13,33

^ais calculated according to the mass production yields and product market prices of jet fuel and by-product naphtha from.³³

^bThe density of TOPs and baled biomass is assumed to be 800 kg/m³ and 100 kg/m³, respectively. Assuming the truck for material transportation has a load limit of 25 Mg with a volume limit of 100 m³. Therefore, the transportation cost for TOPs is assumed to be 40% of the transportation cost of baled biomass.

^c0.6 MW electricity for chopper and dry air blower is saved because the chopping and drying processes are not included in the TOPs-feed biorefinery, and more electricity (10.004 MW) is generated because the power used for drying feedstock is used for electricity generation according to Swanson et al.³⁷ The extra electricity generation is considered as a credit that contributes to a reduction in the variable OPEX compared to the bale-feed biorefinery.

^dThe CAPEX-dependent OPEX cost is calculated as a factor (0.102) of the total CAPEX and thus scales with capacity.

Table 4. Capital expenditure of storage and pretreatment facility (TOPs).⁴⁷

Capacity level of SP	Lower limit capacity of SP s_{lowcap}^l (mg/year)	Upper limit capacity of SP s_{upcap}^l (mg/year)	Variable capital expenditure s_v^l (\$/mg)	Fixed capital expenditure $s_f^{m,l}$ (\$)
$l = 1$	50,000	600,000	47.323	4,909,300
$l = 2$	600,000	1,300,000	32.983	13,037,000
$l = 3$	1,300,000	2,000,000	28.122	19,088,000

Table 5. Capital expenditure of baled biomass-feed gasification-FT biorefinery facility.⁴⁰

Capacity level of biorefinery	Lower limit capacity of biorefinery $f_{lowcap}^{m,l}$ (mg/year)	Upper limit capacity of biorefinery $f_{upcap}^{m,l}$ (mg/year)	Variable capital expenditure $e_v^{m,l}$ (\$/mg biomass)	Fixed capital expenditure $e_f^{m,l}$ (\$)
$l = 1$	50,000	600,000	695.9	72,193,000
$l = 2$	600,000	1,300,000	485.01	191,709,000
$l = 3$	1,300,000	2,000,000	413.54	280,693,000

Table 6. Capital expenditure of TOPs-feed based gasification-FT biorefinery facility (assumed to be 91.5% of the total capital cost for baled biomass feed based FT biorefinery facility).

Capacity level of biorefinery	Lower limit capacity of biorefinery $f_{lowcap}^{m,l}$ (mg/year)	Upper limit capacity of biorefinery $f_{upcap}^{m,l}$ (mg/year)	Variable capital expenditure $e_v^{m,l}$ (\$/mg biomass)	Fixed capital expenditure $e_f^{m,l}$ (\$)
$l = 1$	50,000	600,000	636.75	66,056,000
$l = 2$	600,000	1,300,000	443.79	175,414,000
$l = 3$	1,300,000	2,000,000	378.39	256,835,000

Note: Considering the proper size and low moisture content (1–5%) of TOPs, chopping and drying related equipment are assumed not to be used in the TOPs feed based gasification-FT plant, which contributes to a lower total installed equipment investment compared to the baled biomass feed based gasification-FT plant. A factor of 0.915 as the ratio of the total installed equipment investment without the chopping and drying related equipment to the total installed equipment investment with the chopping and drying related equipment is used to estimate the capital expenditure of the TOPs feed based gasification-FT biorefinery facility. This factor is calculated based on the equipment cost list from Swanson *et al.*³⁷

higher than the criterion were excluded. The final economic optimization was then carried out based on the rest of the grid cells. The breakdown of the curves by biomass category curves indicates that the energy crop-derived jet fuel achieves a much lower GHG emission than the residue-derived jet fuel due to the lower provision GHG emission of energy crops.

Optimal layout under economic optimization

The optimal spatial layouts of the RJF supply chain under least-cost optimization before excluding grid cells under the three scenarios are shown in Fig. 5 while Fig. 6 shows the optimal RJF supply chain layouts under the economic optimization after excluding grids under the three scenarios. There is almost no change in the optimal layout of the supply chain after excluding grid cells compared with the layout before excluding under the Min scenario because only one grid cell was excluded. However, a large number of grid cells locating in the south of the region have been excluded, so the

optimal layouts of the supply chain under the Inter and Max scenarios have changed greatly. The optimal layouts show that all biorefineries are chosen to be at a large scale (1 300 000–2000,000 Mg-year⁻¹ biomass input) to achieve cost reduction by the economies of scale (Table 8). The supply chain configuration tends to be more centralized than distributed according to the quantity of bale-feed biorefineries, which is more than TOPs-feed biorefineries under the Inter and Max scenarios (Table 8). However, the supply chain configuration under the Min scenario is half centralized and half distributed. The difference between scenarios is mainly caused by their different spatial distributions of biomass resource density. The resource density in most regions under the Min scenario is relatively low, thus requires more area to fulfill a large-scale biorefinery that could benefit from the economies of scale and increases the transportation distances from biomass supply sites to the biorefinery. To reduce the transportation cost, a distributed configuration is suggested. In this case, although the capital investment for a bale-feed biorefinery is cheaper than the sum of SP and TOPs-feed

Table 7. GHG emission-related parameters.

Description	Value	Source
Energy allocation factor for jet fuel	0.77 ^a	33
GHG emission during raw biomass (baled) transportation	0.1206 kg CO _{2-eq} /Mg biomass/km	34
GHG emission during pre-processed biomass (TOPs) transportation	0.096 kg CO _{2-eq} /Mg biomass/km	34
GHG emission during SP process	126.336 kg CO _{2-eq} /Mg biomass ^b	35
GHG emission during bale-feed biorefinery process	-9.63 kg CO _{2-eq} /GJ fuel ^c	33
GHG emission during TOPs-feed biorefinery process	-34.84 kg CO _{2-eq} /GJ fuel ^d	33,37

^ais calculated according to the mass production yields and energy contents of jet fuel and by-product naphtha from de Jong *et al.*³³

^bis calculated based on the GHG emission factor (1.128 kg CO_{2-eq}/kWh) of coal-fired electricity produced in China and the net electricity consumption (108.9 kWh/Mg biomass) data from Batidzirai *et al.*³⁵

^cis calculated based on the GHG emission factor (1.128 kg CO_{2-eq}/kWh) of coal-fired electricity produced in China and GHG emission data from de Jong *et al.*³³

^d0.6 MW electricity for chopper and dry air blower is saved because chopping and drying processes are not included in the TOPs-feed biorefinery, and more electricity (10.004 MW) is generated because the power used for drying feedstock is used for electricity generation according to Swanson *et al.*³⁷ This extra electricity generation is regarded as a GHG emission credit that results in a higher negative GHG emission compared to the bale-feed biorefinery.

biorefinery facilities, the advantage of reduced transportation cost of processed biomass outweigh the benefit of the low-priced bale-feed biorefinery. On the other hand, the supply chain prefers a centralized configuration in a region with high resource density.

Economic performance

Figure 7 compares the average unit production costs and their breakdown of RJF production between the economic optimization before and after excluding under the three scenarios. The least average cost after excluding grid cells of the RJF supply chain is calculated to be 24.7, 30.2, and 29.2 \$·GJ⁻¹ with a total RJF production of 19.1, 244.6, and 290.3 PJ under the Min, Inter, and Max scenarios, respectively. There is a slight increase in RJF production cost and a dramatic decrease in total RJF production volume after excluding compared to that before excluding. The cost breakdown shows the visible cost increases in biomass provision, SP, and transportation. The reason for the increase in biomass provision cost is the increase in the share of energy crops after excluding the grid cells that are mostly occupied by agricultural residues that have a higher GHG emission but lower procurement costs than energy crops. The increased SP cost after excluding is caused by the increased quantity of SP, and the increased transportation costs result from the increased transportation distances between sites after excluding grid cells. The biorefinery cost accounts for the majority of the total RJF production cost under the three scenarios,

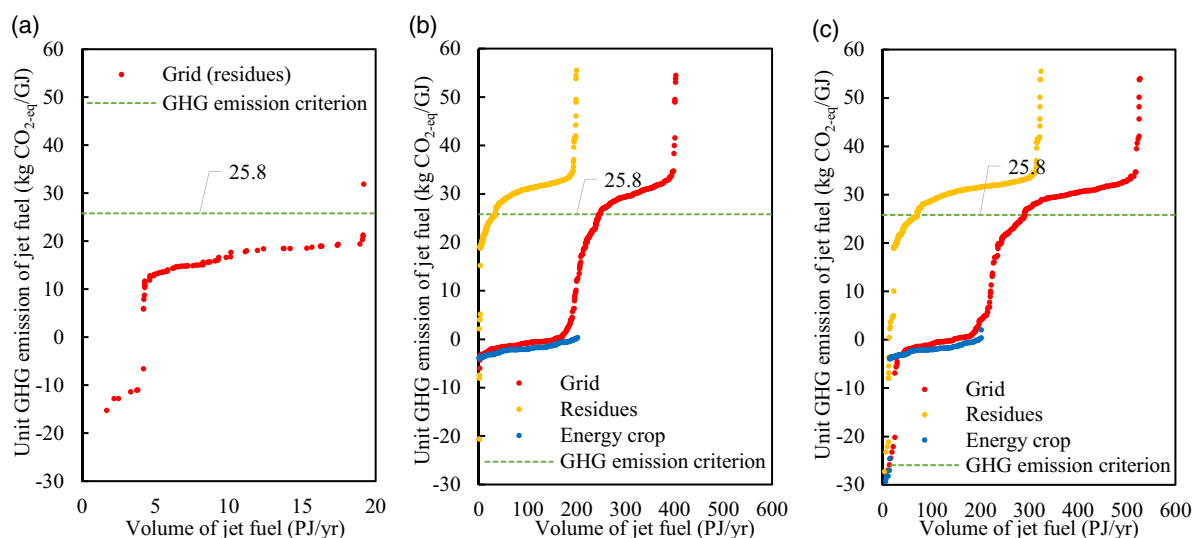


Figure 4. Greenhouse gas emission supply curves on a grid cell basis under environmental optimization for three scenarios: (a) Min; (b) Inter; (c) Max. The green line represents the criterion for excluding grids with a GHG emission higher than 25.8 kg CO_{2-eq}·GJ⁻¹.

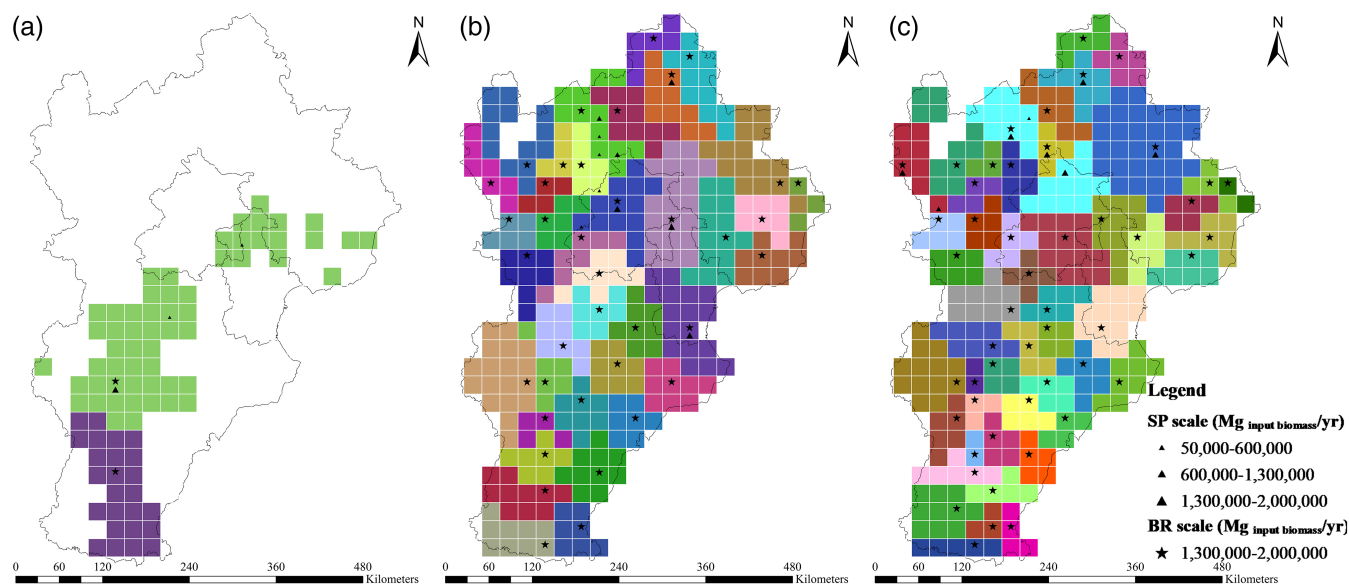


Figure 5. Optimal RJF supply chain layouts under economic optimization before excluding grid cells for the three scenarios: (a) Min; (b) Inter; (c) Max. A same colored area represents one biomass supply region served by storage and pre-processing (SP) or biorefinery (BR) facilities contained within that region. Biorefineries source biomass from SPs or directly from biomass supply sites of the same color. A common colored area where SP appears represents a distributed supply chain configuration, while a common colored area where no SP appears means that there is a centralized supply chain configuration.

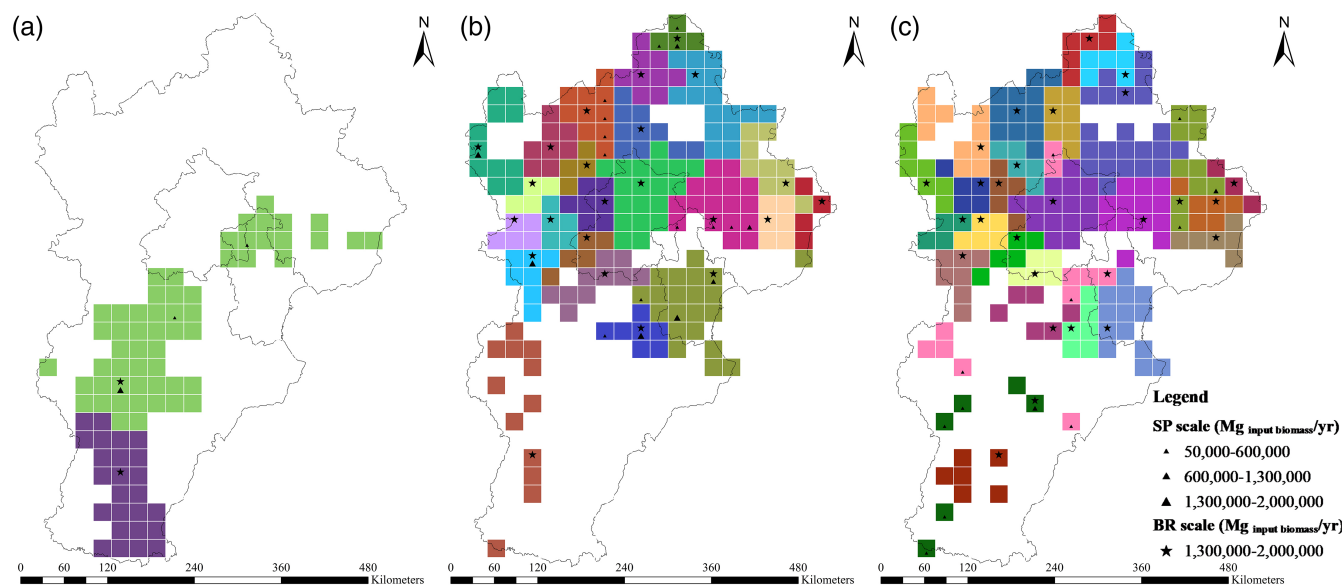


Figure 6. Optimal RJF supply chain layouts under economic optimization after excluding grids with high GHG emission for the three scenarios: (a) Min, (b) Inter, (c) Max. A common colored area represents one biomass supply region served by storage and pre-processing (SP) or biorefinery (BR) facilities contained within that region. Biorefineries source biomass feedstock from SPs or directly from biomass supply sites of the same color. A common colored area where SP appears represents a distributed supply chain configuration, while a common colored area where no SP appears means that there is a centralized supply chain configuration.

followed by biomass provision cost under Inter and Max scenarios (Fig. 7). The biomass provision cost is lower under the Min scenario than the other two scenarios

because the Min scenario does not include energy crops that have a higher procurement cost than residues. The differences in total RJF production costs between scenarios

Table 8. Quantity and scale range of the biomass supply sites, SPs, and biorefineries under economic optimization after excluding grid cells.

	Biomass supply site		SP		Biorefinery	
	Number	Number	Scale range (1000 mg)		Number	Scale range (1000 mg)
Min	81	2	50–600		0	50–600
		0	600–1300		0	600–1300
		1	1300–2000		2	1300–2000
Inter	210	11	50–600		0	50–600
		3	600–1300		0	600–1300
		4	1300–2000		23	1300–2000
Max	212	10	50–600		0	50–600
		2	600–1300		0	600–1300
		0	1300–2000		27	1300–2000

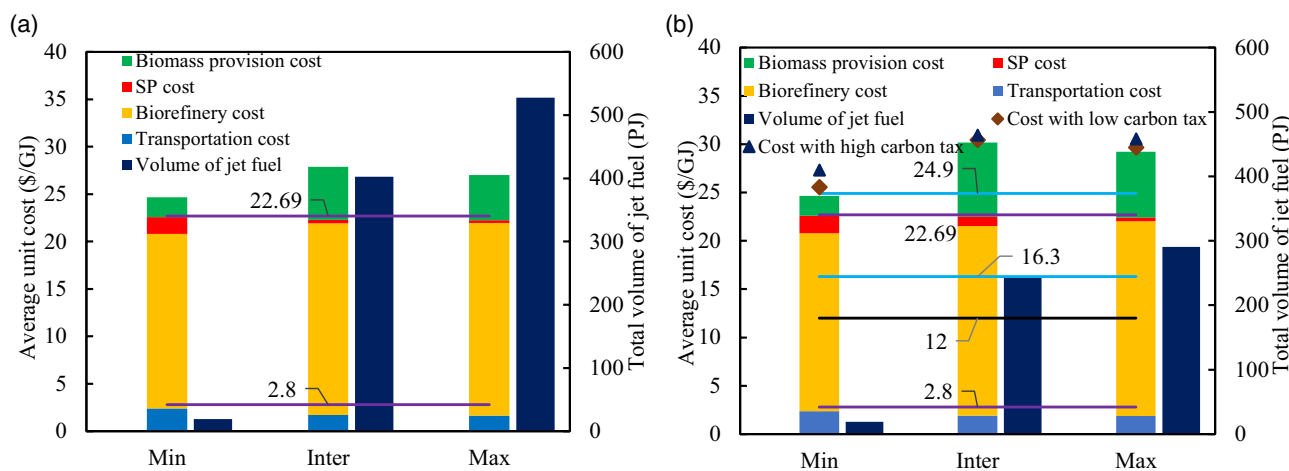


Figure 7. Breakdown of the average unit cost of RJF supply chain and the total volume of jet fuel for three scenarios under cost optimization (a) before excluding grid cells; (b) after excluding grid cells with a GHG reduction potential lower than 70%. The lines in purple represent the up-and-down production costs of fossil jet kerosene with a crude oil price range of 16.5–133.9 \$/barrel from 2006 to 2020. The line in black represents the average production costs of fossil jet kerosene with a 15-year average crude oil price of 70.9 \$/barrel from 2006 to 2020. The lines in blue represent the up-and-down production costs of fossil jet kerosene with a carbon tax ranged from 50 to 150 \$/tonne CO_{2-eq} based on the 15-year average production cost of fossil jet kerosene.

mainly result from the different biomass provision costs of agricultural residues and energy crops. The proportion of SP costs to total costs under the Min scenario (7.3%) is much higher than the other two (3.2% and 1.4% for Inter and Max scenarios, respectively) because the proportion of grid cells served by the distributed configuration under Min scenario is higher than the other two scenarios where the most chosen supply chain configuration is the centralized configuration that does not include an SP facility. Figure 8 shows that there are great variations in RJF production cost between grid cells. The grid cells with high production costs normally have a distribution of expensive energy crops with high resource density.

The lowest cost of RJF production still exceeds the production cost range of fossil jet fuel (2.8–22.7 \$·GJ⁻¹) at a crude oil price range of 16.5–133.9 \$·barrel⁻¹ (with a 15-year average price of 70.9 \$·barrel⁻¹) from 2006 to 2020 (Fig. 7).^{49,50} It is not cost-competitive to fossil jet fuel until the crude oil price hit 145.7, 178.0, and 166.4 \$·barrel⁻¹ under Min, Inter, and Max scenarios, respectively. In comparison with other studies, the costs of FT jet fuel in this study are within the range of 14.9–45.4 \$·GJ⁻¹ from the literature survey.^{12,33,37,40,51–55} The difference compared with the costs of other studies is mainly caused by the different biomass procurement costs used in this study.

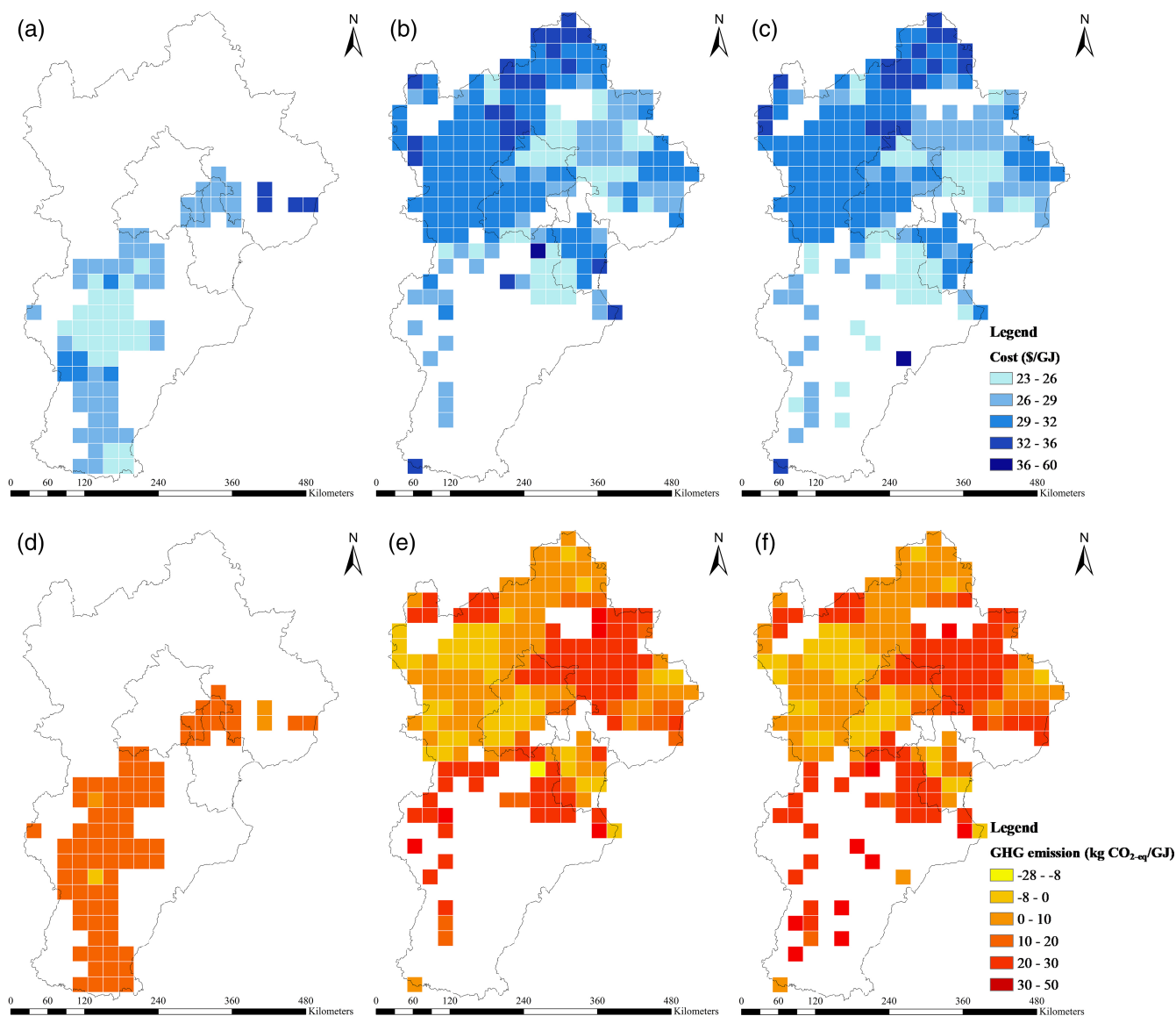


Figure 8. Spatial distributions of RJF supply chain cost and GHG emission on a grid cell basis under least-cost optimization after excluding grid cells for three scenarios: Cost under (a) Min, (b) Inter, and (c) Max; GHG under (d) Min, (e) Inter, and (f) Max.

The cost-supply curves (Fig. 9) depict how much RJF could be supplied annually at certain levels of production cost. For the economic potential, the results show that almost all jet fuel could be obtained at a production cost of less than 35 \$·GJ⁻¹ for Inter and Max scenarios and less than 30 \$·GJ⁻¹ for Min scenario. The breakdown of the cost-supply curve by biomass category indicates that energy crops contribute to most of the biomass feedstock for RJF production but have a high RJF production cost, while agricultural residues achieve a lower RJF production cost but only contribute to a minority of the feedstock under Inter and Max scenarios.

Greenhouse gas emission performance

Figure 10 compares the average unit GHG emissions and their breakdown of RJF production between the economic optimization before and after excluding under the three scenarios. The average unit GHG emissions of RJF production under economic optimization have been significantly reduced by 52% and 47% after excluding grid cells with high GHG emission for Inter and Max scenarios, respectively, whereas almost no change in average unit GHG emission for the Min scenario. The reduction in GHG emissions mainly comes from the reduction in the emission

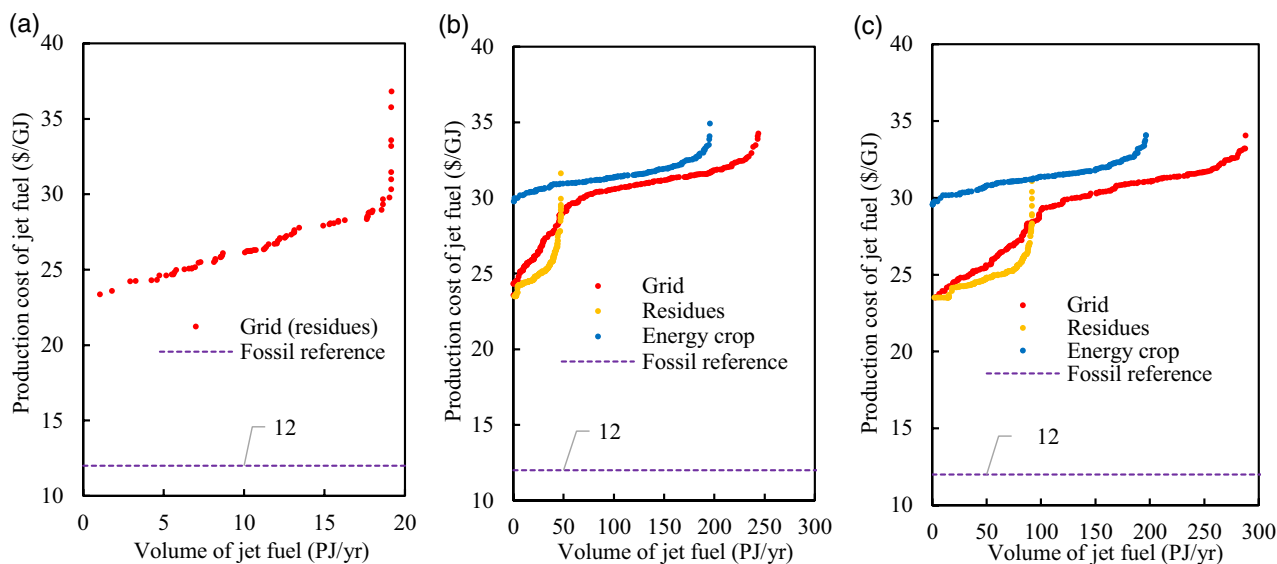


Figure 9. Cost-supply curves on a grid cell basis under economic optimization after excluding grid cells for three scenarios: (a) Min, (b) Inter, and (c) Max. The dotted line in purple represents the average production costs of fossil jet kerosene with a 15-year average crude oil price of 70.9 \$/barrel from 2006 to 2020.

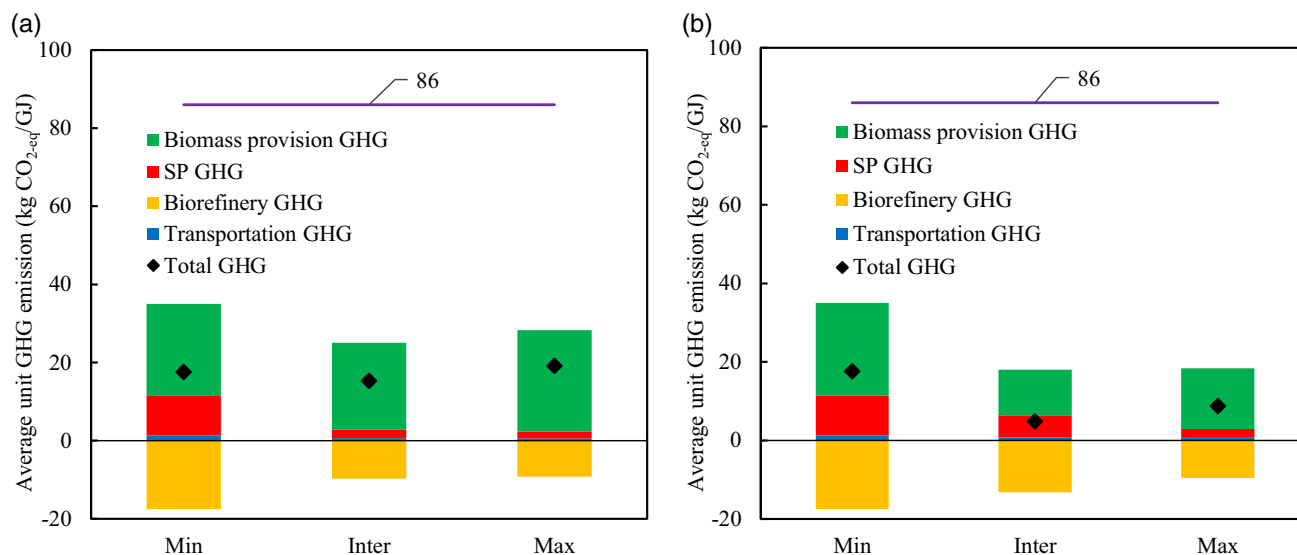


Figure 10. Breakdown of the average unit GHG emission of RJJ supply chain for three scenarios under least-cost optimization: (a) before excluding grid cells; (b) after excluding grid cells with a GHG reduction potential lower than 70%. The line in purple represents the life cycle GHG emission of the fossil jet kerosene.

of biomass provision, which is caused by the increased share of low-emission energy crops after excluding (Fig. 4). The biomass provision emission accounts for the majority of total positive GHG emissions, followed by SP and transportation GHG emissions. The GHG emissions during the biorefinery process are the only negative emissions and make a significant contribution to GHG reduction. There are notable increases in positive GHG emissions during the SP

process and negative GHG emissions during the biorefinery process for Inter and Max scenarios after excluding grid cells with high GHG emission. This because the supply chain configuration after excluding becomes more distributed than before, which contributes to high quantities of SP facility and distributed biorefinery facility that has a stronger negative GHG emission than the centralized biorefinery facility. Figure 8 shows that almost all grid cells have a positive

GHG emission under the Min scenario, while about 20% of the grid cells achieve a negative GHG emission under Inter and Max scenario. The regions with high GHG emission normally do not have distribution or have a low density of energy crops, which is characterized by low-provision GHG emission.

The RJF achieves a reduction of 79.5%, 94.4%, and 89.8% in GHG emission compared to fossil jet fuel ($86 \text{ kg CO}_2\text{-eq}\cdot\text{GJ}^{-1}$) under Min, Inter, and Max scenarios, respectively. If the GHG reduction credit from RJF could be monetized by a carbon tax, the price of RJF could be cost-competitive compared to fossil jet fuel. According to the 15-year average production cost of fossil jet fuel ($12 \text{ \$}\cdot\text{GJ}^{-1}$) from 2006 to 2020, the up and down production costs of fossil jet kerosene with a carbon tax ranged from 50 to 150 $\text{\$/tonne CO}_2\text{-eq}$ were estimated to be 16.3 and 24.9 $\text{\$/GJ}^{-1}$, respectively, which are still cheaper than the production costs of RJF with the same carbon tax (Fig. 7). The price of RJF will not be cost-competitive until the carbon tax reaches 184.9, 224.0, and 222.8 $\text{\$/tonne}^{-1} \text{ CO}_2\text{-eq}$ under Min, Inter, and Max scenarios, respectively.

Comprehensive performance of scenarios

For the Min scenario, there is negligible change in the average unit cost and GHG emission of RJF production between the first-time environmental optimization (before excluding grid cells) and the second time economic optimization (after excluding grid cells), because only one grid cell was excluded. For the Inter and Max scenarios, the dramatic reductions in GHG emissions only result in a small increase in cost, especially for the Inter scenario. The Inter scenario yields the lowest GHG emission but the highest production cost, while the Min scenario yields the lowest production cost but the highest GHG emission, with the Max scenario in between. In comparison with the Max scenario, the Inter scenario has a much lower GHG emission with a negligible higher production cost. Although its total production volume is a little lower than that of the Max scenario, it still accounts for around 62% of the total jet fuel consumption in the Jing-Jin-Ji region in 2050. Therefore, from the perspective of GHG reduction potential, the Inter scenario is the most suitable and realistic for RJF production in the future due to its GHG reduction benefit and the consideration of competing demands of agricultural residues. However, both Inter and Max scenarios do not consider the SOC stock balance of agricultural land. If maintaining the SOC content at 2% or more is a priority, the Min scenario should be seriously considered even though it could only meet 5% of jet fuel demand in the Jing-Jin-Ji region in 2050.

Sensitivity analysis

The GHG emissions estimated in this study exceed the range of $-3\text{--}14 \text{ kg CO}_2\text{-eq}\cdot\text{GJ}^{-1}$ reported on other prior studies.^{12,34,56,57} The difference in GHG emissions is mainly caused by the different input data for biomass provision GHG emission and the methods (energy allocation and displacement methods) used to deal with co-products.

Some GHG emission factors used in this study are facing uncertainties and this may have an impact on the results. One important factor is the GHG emission factor of the product that is used to replace the co-product produced during the biorefinery process. The negative GHG emissions during the biorefinery process were calculated based on the co-product (electricity in this study) production by using a displacement method. The GHG emission credits of the co-product therefore depend on the GHG emission factors of the displaced product. The displaced product used to replace the co-product in this study is coal-fired electricity produced in the Jing-Jin-Ji region, which has a higher GHG emission factor than electricity from other sources, such as biomass co-fired power, hydropower, nuclear power, wind power, and solar power from other regions. To illustrate the impact of using different displaced power on the GHG performance of the supply chain, a sensitivity analysis is carried out with a variation of -50% in the GHG emission factor of the displaced electricity. This study used coal-fired electricity, which has the highest GHG emission factor in China, a positive variation in the GHG emission factor is not considered in this study. Another important factor is that the allocation factor that is used to calculate the GHG emission from agricultural residues at the cultivation stage. The allocation factor used in this study was calculated by the share of mass of crop product and residue. However, the value of residues is uncertain and may fluctuate in the future depending on the residues market. The emission factor of residues will therefore change along with the price of residues if the price is counted in the calculation of the allocation factor. To evaluate the impact of the allocation factor on the GHG emissions result, a sensitivity analysis is conducted with a variation of $\pm 20\%$ in the allocation factor.

The GHG emission factor of the displaced electricity has a great impact on the total GHG emission of the supply chain (Fig. 11). A 50% reduction in the factor results in six times higher total GHG emissions for the Inter scenario, four times higher for the Max scenario, and two-and-a-half times higher for the Min scenario. It indicates that the GHG emission credit from producing extra electricity during the FT process will be significantly reduced with the increase in the share of renewable electricity generation in the future. The residue

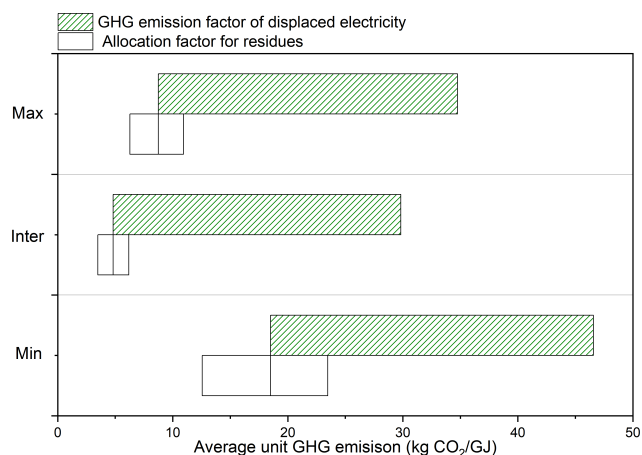


Figure 11. Sensitivity analysis of residues allocation factor and GHG emission factor of displaced electricity.

allocation factor is shown to have a modest impact (25–32% range) on the total GHG emissions.

The production of electricity from the FT process might be reduced by recycling the off-gas to produce more FT liquids instead of combusting the off-gas to generate electricity.⁵⁸ This would maximize the yield of FT liquids and result in a lower production of electricity.⁵⁸ The GHG emission performance would therefore be affected by the improved FT conversion efficiency and the reduced GHG emission credit from net electricity production.

Uncertainty and future research recommendation

This study focuses on the strategic optimization of the supply chain rather than a tactical optimization. Therefore, seasonal variations in biomass supply and the differences in harvest windows of multiple feedstocks are not within the scope of this study. However, it should be noted that the real cost of the supply chain may increase with the inclusion of the storage costs, which result from the short harvest windows of agricultural residues and energy crops. Combining both agricultural residues and energy crops implies larger harvest windows and less storage time, which contributes to lower biomass losses. It is therefore necessary to consider the harvest window and storage cost in a tactical optimization of biofuel supply chain in further studies.

In this work, the procurement costs of agricultural residues were assumed to be the same under scenarios with or without considering competing use. However, the competing demand of agricultural residues for alternative use may have an impact on the selling price of residues from farmers based on market rules. Nevertheless, the extent to which competing demand of agricultural residues affects the selling price is unclear

due to lack of relevant research. In this study, we assumed that all available biomass resources are used to produce as much renewable jet fuel as possible to explore the maximum potential of RJF production. However, the amount of biomass resources used for RJF production depends on future policy and local fuel demand. To explore the impact of different jet fuel demands on the RJF supply chain, and consider the distribution of jet fuel to consumers, it is necessary to carry out the optimization of a complete four-stage supply chain with different replacement rates for renewable jet fuel.

Conclusions

This study developed a GIS-based MILP optimization model to incorporate dual feedstock resources and two supply chain configuration types (centralized and distributed) for economic and environmental optimization of a three-stage lignocellulosic-based biofuel supply chain. A universal three-step optimization approach integrating this model was proposed to design an economically optimal biofuel supply chain strategically on a grid-cell basis on the premise of meeting a certain GHG reduction criterion (70% reduction compared to fossil jet fuel) and maintaining soil health with the assumption that all biomass resources are selected in the biofuel supply chain. A few biomass supply sites would be excluded from the original dataset according to the GHG emission criterion based on the GHG emission performance of each grid cell by the first-step environmental optimization. Then economic optimization was conducted to evaluate the economic and environmental performance including production costs and GHG emission on a grid-cell basis and optimize the decisions.

This approach was applied to optimize a renewable jet fuel supply chain in the Jing-Jin-Ji region in North China at a 25 × 25 km grid cell resolution under different biomass availability (minimum, intermediate, and maximum) for case study. The results show that the differences in procurement costs and GHG emissions between energy crops and agricultural residues have a great impact on the layout of the supply chain. The supply chain configuration tends to be more centralized with large-scale biorefineries when a supply region has an intensive and centralized distribution of resources. Biorefinery-related costs account for the majority of the total production costs; whereas biomass provision and biorefinery-related GHG emissions are the main contributors for the total positive and negative GHG emissions, respectively. The breakdown of cost-supply curves by biomass category indicates that agricultural residue-derived jet fuel achieves lower production costs compared to energy crop-derived jet fuel. Given the great potential of GHG emission

reduction of renewable jet fuel, the production cost of RJF will start to be cost-competitive compared to fossil fuel if carbon tax and crude oil price increased seriously in the future. The Max scenario achieves the highest RJF production that accounts for 73% of the projected demand for jet fuel in the Jing-Jin-Ji region in 2050. The Inter scenario is the most suitable and realistic for RJF production in the future due to its GHG reduction benefit and its consideration of competing demands of agricultural residues. However, if maintaining the SOC content at 2% or more is a priority, the Min scenario should be seriously considered. This study assumed a 70% of reduction in GHG emission compared with conventional jet fuel to be the GHG emission criterion, which is a high-level standard. It should be noted that the GHG emission criterion could be assumed to be any value by policymakers according to the local GHG reduction goals. A lenient GHG reduction standard will allow more biomass resources to be used.

This study provides researchers and industries with a modeling approach to economically optimize the layout of the biofuel supply chain under local biofuel development schemes or regulatory frameworks, especially including GHG emission reduction and soil carbon stock balance goals. It can be adapted to other kinds of biofuel supply chain optimization with different feedstocks and conversion pathways by incorporating related input spatial data, techno-economic, and environmental parameters.

Acknowledgements

This study was partially supported by the China Scholarship Council (CSC), the China National Key Research and Development Plan under Grant Number 2017YFD0700605, and the National Natural Science Foundation of China under Grant Number 31701316.

References

1. Gerssen-Gondelach SJ, Saygin D, Wicke B, Patel MK and Faaij APC, Competing uses of biomass: assessment and comparison of the performance of bio-based heat, power, fuels and materials. *Renew Sustain Energy Rev* **40**:964–998 (2014).
2. Barahira DS, Okudoh VI and Eloka-Eboka AC, Suitability of crop residues as feedstock for biofuel production in South Africa: a sustainable win-win scenario. *J Oleo Sci* **70**:213–226 (2021).
3. IEA. World Energy Outlook 2019. Paris, 2019 <https://webstore.iea.org/download/summary/2467?fileName=Japanese-Summary-WEO2019.pdf>.
4. Zhu X, Li X, Yao Q and Chen Y, Challenges and models in supporting logistics system design for dedicated-biomass-based bioenergy industry. *Bioresour Technol* **102**:1344–1351 (2011).
5. Junginger M, Faaij A, van den Broek R, Koopmans A and Hulscher W, Fuel supply strategies for large-scale bio- energy projects in developing countries: electricity from agricultural and forest residues in north-eastern Thailand fuel supply strategies for large-scale bio-energy projects in developing countries. *Biomass Bioenergy* **21**:259–275 (2001).
6. Inyang V, Anozie A and Odejebi O, Modeling and optimization of Jatropha supply chain for biodiesel production in Nigeria. *Br J Appl Sci Technol* **7**:597–609 (2015).
7. De Meyer A, Cattrysse D, Rasinmäki J and Van Orshoven J, Methods to optimise the design and management of biomass-for-bioenergy supply chains: a review. *Renew Sustain Energy Rev* **31**:657–670 (2014).
8. Sahoo K, Hawkins GL, Yao XA, Samples K and Mani S, GIS-based biomass assessment and supply logistics system for a sustainable biorefinery: a case study with cotton stalks in the Southeastern US. *Appl Energy* **182**:260–273 (2016).
9. Lin T, Rodríguez LF, Shastri YN, Hansen AC and Ting K, GIS-enabled biomass-ethanol supply chain optimization: model development and Miscanthus application. *Biofuels Bioprod Biorefin* **7**:314–333 (2013).
10. Jonker JGG, Junginger HM, Versteegen JA, Lin T, Rodríguez LF, Ting KC *et al.*, Supply chain optimization of sugarcane first generation and eucalyptus second generation ethanol production in Brazil. *Appl Energy* **173**:494–510 (2016).
11. Hu H, Lin T, Wang S and Rodríguez LF, A cyberGIS approach to uncertainty and sensitivity analysis in biomass supply chain optimization. *Appl Energy* **203**:26–40 (2017).
12. Huang E, Zhang X, Rodríguez L, Khanna M, de Jong S, Ting KC *et al.*, Multi-objective optimization for sustainable renewable jet fuel production: a case study of corn stover based supply chain system in Midwestern U.S. *Renew Sustain Energy Rev* **115**:109403 (2019).
13. de Jong S, Hoefnagels R, Wetterlund E, Pettersson K, Faaij A and Junginger M, Cost optimization of biofuel production—the impact of scale, integration, transport and supply chain configurations. *Appl Energy* **195**:1055–1070 (2017).
14. European Parliament and Council. Directive 2009/28/EC of the European Parliament and of the Council of 23 April 2009 on the promotion of the use of energy from renewable sources and amending and subsequently repealing Directives 2001/77/EC and 2003/30/EC (Text with EEA relevance). 2009.
15. Environmental Protection Agency. Regulation of fuels and fuel additives: changes to renewable fuel standard program; Final Rule 2010.
16. Zamboni A, Shah N and Bezzo F, Spatially explicit static model for the strategic design of future bioethanol production systems. 2. Multi-objective environmental optimization. *Energy Fuels* **23**:5134–5143 (2009).
17. You F, Tao L, Graziano DJ and Snyder SW, Optimal design of sustainable cellulosic biofuel supply chains: multiobjective optimization coupled with life cycle assessment and input-output analysis. *AIChE J* **58**:1157–1180 (2012).
18. Santibañez-Aguilar JE, González-Campos JB, Ponce-Ortega JM, Serna-González M and El-Halwagi MM, Optimal planning of a biomass conversion system considering economic and environmental aspects. *Ind Eng Chem Res* **50**:8558–8570 (2011).
19. Malladi KT and Sowlati T, Bi-objective optimization of biomass supply chains considering carbon pricing policies. *Appl Energy* **264**:114719 (2020).
20. Liu Z, Qiu T and Chen B, A study of the LCA based biofuel supply chain multi-objective optimization model with multi-conversion paths in China. *Appl Energy* **126**:221–234 (2014).
21. Liu Y, Zhao R, Wu KJ, Huang T, Chiu ASF and Cai C, A hybrid of multi-objective optimization and system dynamics simulation for straw-to-electricity supply chain management

- under the belt and road initiatives. *Sustain* **10**(3):868 (2018). <https://doi.org/10.3390/su10030868>.
22. Ortiz-Gutiérrez RA, Giarola S and Bezzo F, Optimal design of ethanol supply chains considering carbon trading effects and multiple technologies for side-product exploitation. *Environ Technol* **34**:2189–2199 (2013).
 23. Verstegen JA, Jonker JGG, Karssen D, van der Hilst F, Schmitz O, de Jong SM et al., How a Pareto frontier complements scenario projections in land use change impact assessment. *Environ Model Software* **97**:287–302 (2017).
 24. Monteleone M, Cammerino ARB, Garofalo P and Delivand MK, Straw-to-soil or straw-to-energy? An optimal trade off in a long term sustainability perspective. *Appl Energy* **154**:891–899 (2015).
 25. Andrews SS. Crop Residue Removal for Biomass Energy Production: Effects on Soils and Recommendations 2006.
 26. Chowdhury S, Farrell M, Butler G and Bolan N, Assessing the effect of crop residue removal on soil organic carbon storage and microbial activity in a no-till cropping system. *Soil Use Manage* **31**:450–460 (2015).
 27. Sanderman J and Chappell A, Uncertainty in soil carbon accounting due to unrecognized soil erosion. *Glob Chang Biol* **19**:264–272 (2013).
 28. Ogle SM, Breidt F and Paustian K, Agricultural management impacts on soil organic carbon storage under moist and dry climatic conditions of temperate and tropical regions. *Biogeochemistry* **72**:87–121 (2005).
 29. Zhang B, Xu J, Lin Z, Lin T and Faaij PC, Spatially explicit analyses of sustainable agricultural residue potential for bioenergy in China under various soil and land management scenarios. *Renew Sustain Energy Rev* **137**:110614 (2021).
 30. Zhang B, Hastings A, Clifton-Brown JC, Jiang D and Faaij APC, Spatiotemporal assessment of farm-gate production costs and economic potential of *Miscanthus × giganteus*, *Panicum virgatum* L., and *Jatropha* grown on marginal land in China. *GCB Bioenergy* **12**:310–327 (2020).
 31. Towler G and Ray S, *Chemical engineering design: principles, practice and economics of plant and process design*, Second edn. Elsevier Ltd: Oxford, UK (2012).
 32. Zhang B, Hastings A, Clifton-Brown JC, Jiang D and Faaij APC, Modeled spatial assessment of biomass productivity and technical potential of *Miscanthus × giganteus*, *Panicum virgatum* L., and *Jatropha* on marginal land in China. *GCB Bioenergy* **12**:328–345 (2020).
 33. de Jong S, Hoefnagels R, Faaij A, Slade R, Mawhood R and Junginger M, The feasibility of short-term production strategies for renewable jet fuels - a comprehensive techno-economic comparison. *Biofuels Bioprod Biorefin* **9**:778–800 (2015).
 34. De Jong S, Antonissen K, Hoefnagels R, Lonza L, Wang M, Faaij A et al., Life-cycle analysis of greenhouse gas emissions from renewable jet fuel production. *Biotechnol Biofuels* **10**:1–18 (2017).
 35. Batidzirai B, Mignot APR, Schakel WB, Junginger HM and Faaij APC, Biomass torrefaction technology: techno-economic status and future prospects. *Energy* **62**:196–214 (2013).
 36. Meerman JC, Ramírez A, Turkenburg WC and Faaij APC, Performance of simulated flexible integrated gasification polygeneration facilities. Part A: a technical-energetic assessment. *Renew Sustain Energy Rev* **15**:2563–2587 (2011).
 37. Swanson RM, Platon A, Satrio JA and Brown RC, Techno-economic analysis of biomass-to-liquids production based on gasification scenarios. *ACS Natl Meet B Abstr* 59–62 (2009).
 38. Ahmad AA, Zawawi NA, Kasim FH, Inayat A and Khasri A, Assessing the gasification performance of biomass: a review on biomass gasification process conditions, optimization and economic evaluation. *Renew Sustain Energy Rev* **53**:1333–1347 (2016).
 39. Zhang W, Automotive fuels from biomass via gasification. *Fuel Process Technol* **91**:866–876 (2010).
 40. Zhu Y, Tjokro Rahardjo S, Valkenburg C, Snowden-Swan L, Jones S and Machinal M, *Techno-economic analysis for the thermochemical conversion of biomass to liquid fuels*. Richland, Washington (2011).
 41. Elgowainy A, Han J, Cai H, Wang M, Forman GS and Divita VB, Energy efficiency and greenhouse gas emission intensity of petroleum products at U.S. Refineries. *Environ Sci Technol* **48**:7612–7624 (2014).
 42. Zang H, Blagodatskaya E, Wen Y, Xu X, Dyckmans J and Kuzyakov Y, Carbon sequestration and turnover in soil under the energy crop *Miscanthus*: repeated 13C natural abundance approach and literature synthesis. *GCB Bioenergy* **10**:262–271 (2018).
 43. Ledo A, Smith P, Zerihun A, Whitaker J, Vicente-Vicente JL, Qin Z et al., Changes in soil organic carbon under perennial crops. *Glob Chang Biol* **26**:4158–4168 (2020).
 44. Hu Y, Schäfer G, Duplay J and Kuhn NJ, Bioenergy crop induced changes in soil properties: a case study on *Miscanthus* fields in the upper Rhine region. *PLoS One* **13**:1–15 (2018).
 45. McCalmont JP, Hastings A, McNamara NP, Richter GM, Robson P, Donnison IS et al., Environmental costs and benefits of growing *Miscanthus* for bioenergy in the UK. *GCB Bioenergy* **9**:489–507 (2017).
 46. 1:1,000,000 National Basic Geographical Database. Natl Cat Serv Geogr Inf 2017. <http://www.webmap.cn/commres.do?method=result100W> (Accessed 12 Aug 2020).
 47. Bergman PCA, Boersma AR, Zwart RWR, Kiel JHA. *Torrefaction for biomass co-firing in existing coal-fired power stations*. Energy Centre of Netherlands, Report No. ECN-C-05-013. Utrecht, the Netherlands (2005). <http://www.senternovem.nl>.
 48. Felten D, Fröba N, Fries J and Emmerling C, Energy balances and greenhouse gas-mitigation potentials of bioenergy cropping systems (*Miscanthus*, rapeseed, and maize) based on farming conditions in Western Germany. *Renew Energy* **55**:160–174 (2013).
 49. IEA. Production cost and break-even crude oil price for SAFs compared with fossil jet kerosene, 2019. Paris, 2019. <https://www.iea.org/data-and-statistics/charts/production-cost-and-break-even-crude-oil-price-for-safs-compared-with-fossil-jet-kerosene-2019-2>.
 50. IEA. Average key crude oil spot prices, June 1996–June 2020. Paris, 2020 <https://www.iea.org/data-and-statistics/charts/average-key-crude-oil-spot-prices-june-1996-june-2020>.
 51. Meerman JC, Ramírez A, Turkenburg WC and Faaij APC, Performance of simulated flexible integrated gasification polygeneration facilities, part B: economic evaluation. *Renew Sustain Energy Rev* **16**:6083–6102 (2012).
 52. Atsonios K, Kougioumtzis MA, Panopoulos KD and Kakaras E, Alternative thermochemical routes for aviation biofuels via alcohols synthesis: process modeling, techno-economic assessment and comparison. *Appl Energy* **138**:346–366 (2015).
 53. Haarlemmer G, Boissonnet G, Imbach J, Setier PA and Peduzzi E, Second generation BtL type biofuels - a production cost analysis. *Energy Environ Sci* **5**:8445–8456 (2012).

54. Tunå P and Hulteberg C, Woody biomass-based transportation fuels - a comparative techno-economic study. *Fuel* **117**:1020–1026 (2014).
55. Anex RP, Aden A, Kazi FK, Fortman J, Swanson RM, Wright MM *et al.*, Techno-economic comparison of biomass-to-transportation fuels via pyrolysis, gasification, and biochemical pathways. *Fuel* **89**:S29–S35 (2010).
56. Wang W-C, Tao L, Markham J, Zhang Y, Tan E, Batan L *et al.*, Review of biojet fuel conversion technologies. National Renewable Energy Laboratory, USA (2016). <https://www.nrel.gov/docs/fy16osti/66291.pdf>.
57. Stratton RW, Wong HM and Hileman JI, Quantifying variability in life cycle greenhouse gas inventories of alternative middle distillate transportation fuels. *Environ Sci Technol* **45**:4637–4644 (2011).
58. Tijmensen MJA, Faaij APC, Hamelinck CN and Van Hardeveld MRM, Exploration of the possibilities for production of Fischer Tropsch liquids and power via biomass gasification. *Biomass Bioenergy* **23**:129–152 (2002).



Bingquan Zhang

Dr Bingquan Zhang is a postdoctoral associate at Yale School of Environment, Yale University. His research is at the intersection between system modeling, environmental assessment, and economic analysis of bioenergy, bio-based chemicals, and materials. His research interest is the systems analysis of bio-based product supply chains starting from land-use change to final consumption.



Changqiang Guo

Dr Changqiang Guo is a postdoctoral fellow in the College of Biosystems Engineering and Food Science, Zhejiang University. His research interests include supply-chain optimization, sustainable development, and environmental protection.



Tao Lin

Dr. Tao Lin is ZJU-100 professor at the College of Biosystems Engineering and Food Science, Zhejiang University. His research interests include agricultural systems analysis, agricultural big data and machine intelligence, and decision support systems.



André P.C. Faaij

André P.C. Faaij is director of science of TNO Energy Transition. He combines this position with part-time chairs as Distinguished Professor Energy System Analysis at the University of Groningen (RUG) and Utrecht University (UU). Ongoing research covers energy system integration questions and modeling, industrial transformation, transition processes towards low-carbon energy systems, and related innovation and policy questions.